

Collisional and collisionless expansion of Yukawa balls

Alexander Piel*

IEAP, Christian-Albrechts-Universität, D-24098 Kiel, Germany

John A. Goree

Department of Physics and Astronomy, The University of Iowa, Iowa City, Iowa 52242 USA

(Received 20 September 2013; published 10 December 2013)

The expansion of Yukawa balls is studied by means of molecular dynamics simulations of collisionless and collisional situations. High computation speed was achieved by using the parallel computing power of graphics processing units. When the radius of the Yukawa ball is large compared to the shielding length, the expansion process starts with the blow-off of the outermost layer. A rarefactive wave subsequently propagates radially inward at the speed of longitudinal phonons. This mechanism is fundamentally different from Coulomb explosions, which employ a self-similar expansion of the entire system. In the collisionless limit, the outer layers carry away most of the available energy. The simulations are compared with analytical estimates. In the collisional case, the expansion process can be described by a nonlinear diffusion equation that is a special case of the porous medium equation.

DOI: [10.1103/PhysRevE.88.063103](https://doi.org/10.1103/PhysRevE.88.063103)

PACS number(s): 52.27.Lw, 52.27.Gr, 52.35.-g, 79.77.+g

I. INTRODUCTION

Yukawa balls are spherical objects containing several hundred particles that interact by shielded Coulomb fields. They can be formed using polymer particles of micrometer size in a radio frequency (rf) discharge, which provides particle charging and confinement in a suitable potential trap [1,2]. The particles carry large surface charges ($q = -10,000 e \dots -50,000 e$) and can be in a strongly coupled state, in which the particles arrange themselves in a structure of nested spherical shells [3,4]. Yukawa balls have been used to study structural and dynamical properties of strongly coupled finite clusters [5–8], or phase transitions in such systems [9–11].

The free expansion of a densely packed cloud of microparticles had already been observed in very early experiments with “complex plasmas” [12]. A complex (or dusty) plasma is a mixture of solid microparticles, electrons, ions, and gas [13]. The microparticles accumulate a large negative charge by absorbing some of the electrons, and they repel each other by screened Coulomb forces. A rapid expansion of this microparticle cloud occurred after the plasma discharge that provides the confining potential trap was switched off.

A model for such a situation in the plasma afterglow, in which the charge on the microparticles changes with time, was reported in Ref. [14]. The authors discuss two situations: (1) At low gas pressure the plasma density decays rapidly and the shielding of the microparticles is effectively switched off, which leads to a Coulomb explosion of the microparticles, which still carry their initial negative charge. (2) At high gas pressure, the electron temperature, which determines the charge on the microparticle, drops rapidly while the plasma density decays more slowly. In this case, the screening of the interparticle forces prevails in the afterglow.

Experiments on the expansion of Yukawa balls are still sparse. Recently, the expansion of an initially compressed cloud of microparticles in a steady-state plasma environment was studied experimentally in Ref. [15]. There, a cloud of microparticles was originally confined deep in the sheath of

a parallel-plate rf discharge by means of a small secondary rf plasma. After turning the secondary plasma off, the particles were lifted vertically by the electric field of the sheath and expanded horizontally under their mutual repulsion. The particle motion was friction-dominated. The particle charge was not constant but depended critically on the position in the sheath, rising from $|q| = 900 e$ at the instant of release to nearly $3000 e$ at the final vertical position. Hence, the rising charge increased the repulsive force during the expansion process, which complicates the analysis.

On the other hand, very general analytical models for the expansion of Coulomb systems in plane, cylindrical, and spherical geometry were recently discussed in Ref. [16].

Outside the field of complex plasmas, Coulomb explosions are used to study the structure of large molecules and clusters. This can be done experimentally by impacting them at high speed upon a thin foil [17]. The term “Coulomb explosions” has also been used to describe the acceleration of protons or heavy ions away from a plasma that is suddenly formed by ultraintense laser-plasma interactions; see, e.g., Refs. [18–21].

The present article is not aimed at the analysis of a particular experiment. Rather, the expansion of Yukawa balls is discussed in very general terms. The phenomenon is studied by molecular dynamics simulations, which are compared with analytical models. Only Yukawa balls in a disordered (liquid or glassy) state are considered to exclude correlation effects from the crystalline order and to facilitate the comparison with mean-field models. It is shown that there are fundamental differences in the expansion mechanism of Yukawa and Coulomb systems. Section II summarizes the properties of Coulomb explosions. In Sec. III the principle of Yukawa expansion is demonstrated in a plane stratified system. The implementation of the Langevin molecular dynamics code is described in Sec. IV. The expansion of collisionless Yukawa balls is demonstrated in Sec. V. The influence of collisions is discussed in Sec. VI, where, in addition, a model in terms of a nonlinear diffusion equation is introduced. Appendix A gives a derivation of the sound speed in a system of stratified Yukawa planes. In Appendix B the potential and electric field for several spherical geometries of Yukawa matter are derived in

*piel@physik.uni-kiel.de

the mean-field approximation, among them Yukawa bubbles, Yukawa balls, and Yukawa cavities.

II. COULOMB EXPLOSIONS

Analytical solutions for the collisionless expansion of a homogeneously charged sphere were discussed before in Refs. [22–24]. We give here a simplified derivation to illustrate the differences between Coulomb and Yukawa systems and to introduce collisions [16].

Consider a Coulomb ball of radius R that is homogeneously filled with point-like particles of charge q and mass m . The initial number density of the particles is n_0 and the particles interact pairwise by repulsive Coulomb potentials. For times $t < 0$, this arrangement of particles is assumed to be confined in a potential trap, which is switched off at $t = 0$. An initially homogeneous situation can be generated in a parabolic confining potential [4].

Let us now consider the dynamics of a thin shell of radius $r(t)$, which has the initial radius $r(0) = r_0 < R$ and thickness $\Delta r \ll r_0$. The volume of the sphere bounded by this shell contains the total electric charge $Q(r_0) = (4\pi/3)r_0^3 n_0 q$. The radial electric field at r_0 reads

$$E(r_0) = \frac{Q(r_0)}{4\pi\epsilon_0 r_0^2} = \frac{1}{3} \frac{n_0 q}{\epsilon_0} r_0. \quad (1)$$

Then the initial radial acceleration of a test particle in the considered shell can be written as

$$a(0) = \frac{q}{m} E(r_0) = \frac{1}{3} \omega_0^2 r_0, \quad (2)$$

with the characteristic frequency $\omega_0 = (n_0 q^2 / \epsilon_0 m)^{1/2}$. Despite its similarity to the plasma frequency, ω_0 here denotes a characteristic growth rate for the unstable system. The radial acceleration of the entire shell is the same as that of the test particle since the shell has the same q/m ratio as the test particle.

Because the acceleration increases with the radius, the nesting of the individual shells will be preserved during the expansion. In particular, the total charge $Q(r_0)$ becomes a conserved quantity for the considered shell, although the charge density inside the sphere decreases. At a later time, when this shell has expanded to a radius $r(t)$, the equation of motion becomes

$$\frac{d^2 r}{dt^2} = \frac{1}{3} \omega_0^2 \frac{r_0^3}{r^2} - \gamma \frac{dr}{dt}, \quad (3)$$

with the friction coefficient γ .

Setting $\rho = r/r_0$, $\tau = \omega_0 t$, we obtain the universal equation of motion for the shells of a Coulomb ball:

$$\frac{d^2 \rho}{d\tau^2} = \frac{1}{3\rho^2} - \frac{\gamma}{\omega_0} \frac{d\rho}{d\tau}. \quad (4)$$

Since this equation only depends on the parameter $\nu = \gamma/\omega_0$, all shells perform a self-similar expansion. Therefore, a characteristic feature of an expanding Coulomb ball will be the preservation of its initial homogeneous density profile during the expansion. For $\nu = 0$, the differential Eq. (4) has the solution

$$\sqrt{\rho(\rho-1)} + \operatorname{arctanh} \sqrt{\frac{\rho-1}{\rho}} = \sqrt{\frac{2}{3}} \tau. \quad (5)$$

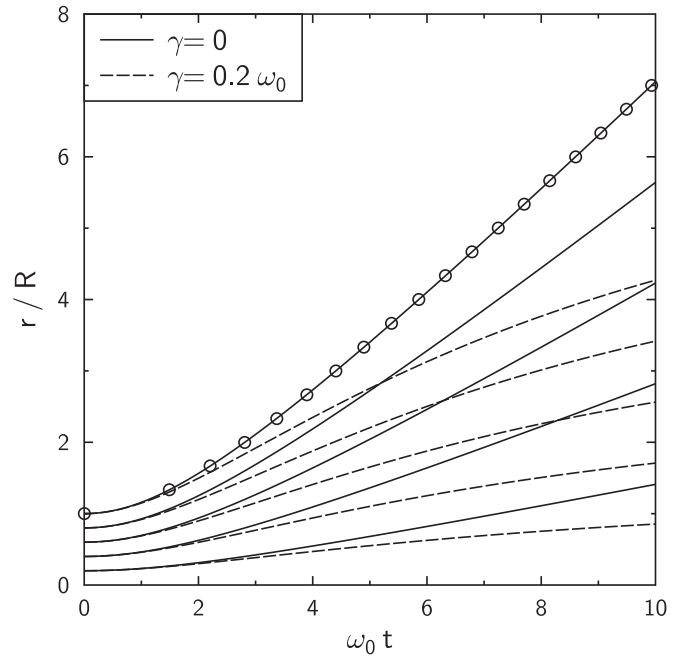


FIG. 1. Self-similar expansion of a Coulomb ball in the collisionless and collisional case by numerical integration of Eq. (4). The circles represent the analytical result Eq. (5).

The self-similar expansion of five representative shells is shown in Fig. 1. The shells were initially spaced equidistantly within the radius R . The curves were obtained by a numerical integration of Eq. (3) for the collisionless case $\gamma = 0$ and for a typical value found in experimental situations, $\gamma/\omega_0 = 0.2$. The self-similarity of the expansion process can be seen in both cases. For the collisionless case, the analytical solution [Eq. (5)] for $\rho_0 = 1$ is superimposed (open circles).

III. EXPANSION OF YUKAWA PARTICLES FILLING A HALFSPACE

Shielded Coulomb interaction is described by a Yukawa (or Debye) potential

$$\Phi_Y(r_{ij}) = \frac{q}{4\pi\epsilon_0 r_{ij}} \exp\left(-\frac{r_{ij}}{\lambda}\right), \quad (6)$$

which depends on the distance r_{ij} of a particle pair (i, j) and contains the shielding length λ . The finite range of this interaction force is the reason for a completely different mechanism of expansion. In order to avoid geometrical complications that arise in spherical symmetry, we first consider a plane geometry, in which the half-space $z < 0$ is homogeneously filled with Yukawa particles of charge q and mass m at a number density n_0 . This system can be considered as a stack of individual thin layers of finite thickness $\Delta z \ll \lambda$.

For a numerical treatment of the problem, we replace each layer by an infinitesimally thin “sheet” in the middle of each layer, which carries a surface charge density $\sigma = n_0 \Delta z$. These sheets have initially an equal spacing Δz and are infinitely large in the lateral directions. The electric field produced by one of these sheets, which is located at position z_k , is given by

$$E(z) = \operatorname{sgn}(z - z_k) \frac{\sigma}{2\epsilon_0} \exp\left(-\frac{|z - z_k|}{\lambda}\right). \quad (7)$$

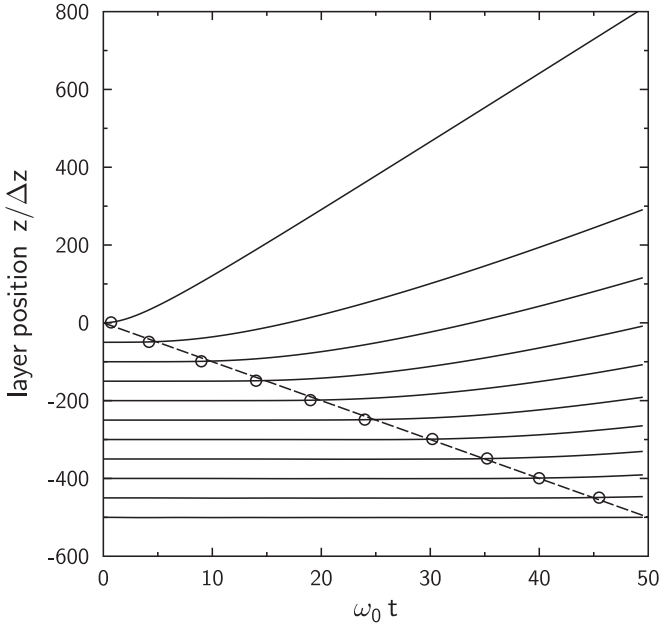


FIG. 2. Expansion of a half-space filled with Yukawa particles for $\Delta z = 0.1\lambda$ and 500 mobile sheets. The circles mark the time when a sheet has been displaced by Δz from its original position. The dashed line represents the sound speed $\omega_0\lambda$.

The equation of motion for such a sheet at position z_n is given by the forces exerted from all other sheets at $z_k = -k \Delta z$ above and below the considered sheet, namely

$$\ddot{z}_n = \frac{1}{2}\omega_0^2\Delta z \left[\sum_{k=n+1}^{\infty} \exp\left(-\frac{|z_n - z_k|}{\lambda}\right) - \sum_{k=0}^{n-1} \exp\left(-\frac{|z_n - z_k|}{\lambda}\right) \right]. \quad (8)$$

The numerical solution of Eq. (8) is performed for a set of 500 mobile sheets ($k = 0 \dots 499$) and by including the force from immobile sheets $k = 500 \dots \infty$ in terms of an integral. The equation of motion of the 500 interacting sheets is solved by a fourth-order Runge-Kutta algorithm. The dynamical evolution of the sheets is shown in Fig. 2, where every 50th sheet is shown. Here, a sheet spacing $\Delta z = 0.1\lambda$ was chosen.

The striking result is that the outermost layer blows off much faster than the other layers. Further, the inner layer apparently begin their expansion only after a delay time. These “starting times” are marked by small circles and are defined as the time at which the considered sheet has been displaced by Δz from its original position. This effect can be understood by comparing these times with the propagation of a longitudinal wave, which has a group velocity $v_g = \omega_0\lambda$ (dashed line). The proper dispersion relation for a set of coupled equidistant charge sheets is shortly derived in the Appendix. A nearly identical group velocity for long-wavelength modes was reported in the frame of the QLCA-treatment of Yukawa particles in Ref. [25].

The mechanism behind this delayed detachment can be explained as follows: Initially, sheets that are deeper than a shielding length λ inside the system are essentially in a force

balance with their neighbors above and below. As soon as the rarefactive wave reaches the position of the considered sheet, this force balance is destroyed and a net force pushes this sheet upwards. In the end, a cascade of delayed detachments describes the expansion of the Yukawa halfspace. These arguments hold for any finite value of λ and the choice of the ratio $\Delta z/\lambda$ only affects the numerical accuracy.

On the other hand, the transition from a Yukawa system to a Coulomb system can be performed by taking the limit $\lambda \rightarrow \infty$. The effect on the speed of the expansion process can be seen from the electric field at the surface of the half-space, which is given in the mean-field approximation by

$$E_z(0) = \frac{n_d q_d}{2\epsilon_0} \lambda. \quad (9)$$

The electric field increases with λ and in the end leads to the well-known Coulomb singularity. Therefore, the discussion will be shifted to finite spherical clusters in the following.

IV. MOLECULAR DYNAMICS SIMULATIONS

In this section we describe the simulation code, which is used to study the collisionless and collisional expansion of Yukawa spheres. The artificial aspects of the stratified layer model in Sec. III, namely the mean-field approximation and the grouping into representative “sheets” can be overcome by molecular dynamics (MD) simulations that take the correct Yukawa interaction force between all particles into account.

The fundamental difference between Coulomb and Yukawa systems is the fact that for a spherical shell the electric field due to Coulomb interaction vanishes inside the shell, whereas for Yukawa interaction it does not.

For later reference, the analytical results for the potential and electric field of spherical Yukawa systems are compiled in Appendix B. Yukawa bubbles, solid Yukawa spheres, and spherical cavities in Yukawa matter are considered. The potential and electric field at the surface of a homogeneous Yukawa ball are needed for discussing the energy of the surface layer. The potential and field inside a Yukawa cavity provide the confinement of a homogeneous start configuration in the simulation.

The expansion of a Yukawa ball is studied by filling a sphere of radius R homogeneously with Yukawa particles. This filling procedure uses random positions but rejects all new particles that come closer than $1.1a_{WS}$ to any of the previously injected particles. This procedure results in a weak excess of potential energy over the ground state, which is typically 5% of the total potential energy.

In the collisionless limit, the motion of each individual particle is calculated using a Verlet algorithm with the actual Yukawa forces obtained from all pair interactions in the cloud of particles. The force calculation is based on a modified N -body routine [26] that is executed on an NVIDIA graphics card (GTX 660Ti) by means of the CUDA extension of the C-language. A total of $N = 2^{16}$ particles are used in this calculation. Typically, a run with 1000 time steps and single-precision arithmetic takes 3 minutes with an 80% share of GPU time.

For the numerical simulation we use normalized quantities for time $\tau = \omega_0 t$, radius $x = r/R$, and shielding parameter

$\kappa = R/\lambda$. Then, the equation of motion for particle i under the action of $(N - 1)$ other shielded particles in the collisionless limit becomes

$$\frac{d^2 \vec{x}_i}{d\tau^2} = \frac{1}{3N} \sum_{j \neq i} \frac{(1 + \kappa x_{ij})}{x_{ij}^3} e^{-\kappa x_{ij}} (\vec{x}_i - \vec{x}_j), \quad (10)$$

with $x_{ij} = |\vec{x}_i - \vec{x}_j|$. This problem has only two parameters, the total number N of particles and the shielding factor R/λ .

In addition to the collisionless MD simulation, we will also use a collisional simulation taking into account two effects of neutral gas collisions with the microparticles, i.e., a random force from gas molecules impinging on them and a frictional force. The latter has the form $-\nu d\vec{x}_i/dt$. For our collisional simulation, we include these two forces using the Langevin-MD method with the Brünger-Brooks-Karplus (BBK) algorithm [27]:

$$\begin{aligned} \vec{x}(t + \Delta t) = & \vec{x}(t) + \frac{1 - \frac{\nu}{2} \Delta t}{1 + \frac{\nu}{2} \Delta t} [\vec{x}(t) - \vec{x}(t - \Delta t)] \\ & + \frac{(\Delta t)^2}{1 + \frac{\nu}{2} \Delta t} [\vec{a}(t) + \vec{L}(t)]. \end{aligned} \quad (11)$$

Here, $\nu = \gamma/\omega_0$ is the normalized friction frequency, $\vec{a}(t)$ the acceleration by the other particles, and $\vec{L}(t) = L_0 \zeta(t)$ is the Langevin acceleration, which involves independent Gaussian random processes $\zeta(t)$ with zero mean and unit variance for each of the coordinates. The standard expression for the Langevin acceleration, $L_0 = [2\gamma k_B T / (m \Delta t)]^{1/2}$ reads in normalized units:

$$L_0 = \left(\frac{2}{3} N^{-2/3} \Gamma^{-1} \frac{\nu}{\Delta \tau} \right)^{1/2}. \quad (12)$$

The coupling factor $\Gamma = q^2 / (4\pi \epsilon_0 a_{\text{WS}} k_B T)$ takes the role of the (inverse) temperature in these normalized units. $a_{\text{WS}} = N^{-1/3} R$ is the Wigner-Seitz radius.

A final remark concerns the proper initial condition for the simulation. The simplest approach, namely to fill the simulation sphere with Yukawa particles at random positions, leads to an often unwanted high electrostatic energy in some particle pairs, which appear as ‘‘hot’’ particles afterwards. This phenomenon is known as disorder-induced heating in the context of ultracold photoionized plasmas (see, e.g., Refs. [28,29]). For careful investigations of the conversion from potential to kinetic energy we seek to minimize these initial correlations.

Using the BBK algorithm, a well-defined start configuration can be established by confining the N discrete simulation particles in the potential well of a cavity of Yukawa matter [see Eq. (B10)] and letting the system relax to a state with prescribed value of Γ . The cavity radius is chosen as $R + 0.5a_{\text{WS}}$. A spatially homogeneous filling is obtained for a liquid state with $\Gamma = 3$. For this starting condition, the system has a similar excess energy as with the random filling. For large values of the coupling factor, $\Gamma = 200$, the excess potential energy is negligible, but a distinct outer shell is formed, which is induced by the confining electric field that acts at the surface. The expansion process is started by suddenly switching the confining potential off.

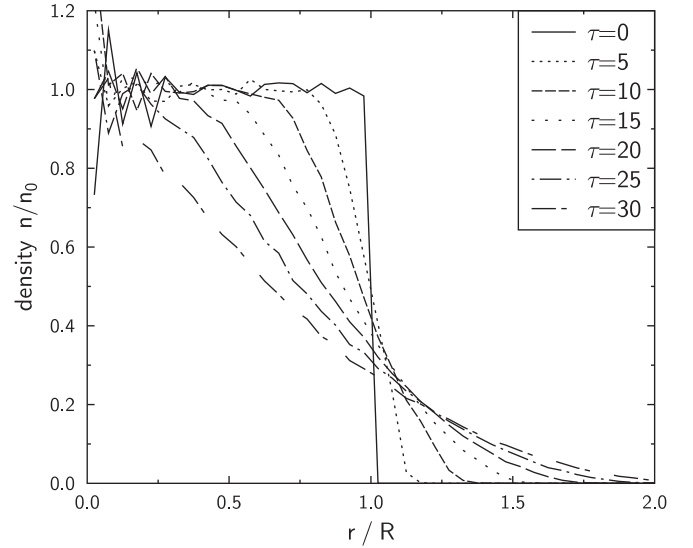


FIG. 3. Short-time expansion of a Yukawa ball ($N = 2^{16}$, $R/\lambda = 40.3$). The inner part of the Yukawa ball maintains its unperturbed homogeneous density while the rarefaction wave propagates radially inwards.

V. COLLISIONLESS EXPANSION OF A YUKAWA BALL

In order to see the delayed blow-off effect of a Yukawa ball, we consider large spheres with $R/\lambda \gg 1$. Experimental situations for Yukawa balls in many cases have a Wigner-Seitz radius that is comparable with the shielding length, $a_{\text{WS}}/\lambda \approx 1$. When we restrict the discussion to this special case, the number of particles inside the simulation sphere defines the ratio R/λ . For $N = 2^{16}$ particles, this corresponds to $R/a_{\text{WS}} = N^{1/3} = 40.3$, which gives the desired large sphere radius.

In this section we use the collisionless MD simulation, which solves Eq. (10). An external confining force that previously provided a force equilibrium is assumed to be turned off at time $\tau = \omega_0 t = 0$. We record the profiles of the energy and density of the microparticles to study how they develop in the expansion.

Density profiles are calculated by sorting the particle positions into radial bins of width Δx and using the proper volume of the shell of finite thickness. The normalized density profile then is $n_k/n_0 = (1/3N)N_k/[k(k+1) + 1/3]\Delta x^3$ for N_k particles in bin k . Near the origin of the sphere, the resulting density values show fluctuations, which are a tribute to the small number of particles in the central bins.

A. Short-time evolution of the density profile

An example for the early expansion phase of such a Yukawa ball is shown in Fig. 3. These results and those shown in Figs. 4–6 are from our collisionless MD simulation for $N = 2^{16}$.

The short-time expansion of the Yukawa ball is governed by the inwards propagating rarefactive wave. Note that the inner part of the density profile remains homogeneous until the rarefactive wave has reached that position. When the rarefactive wave reaches the center, the density profile becomes almost triangular.

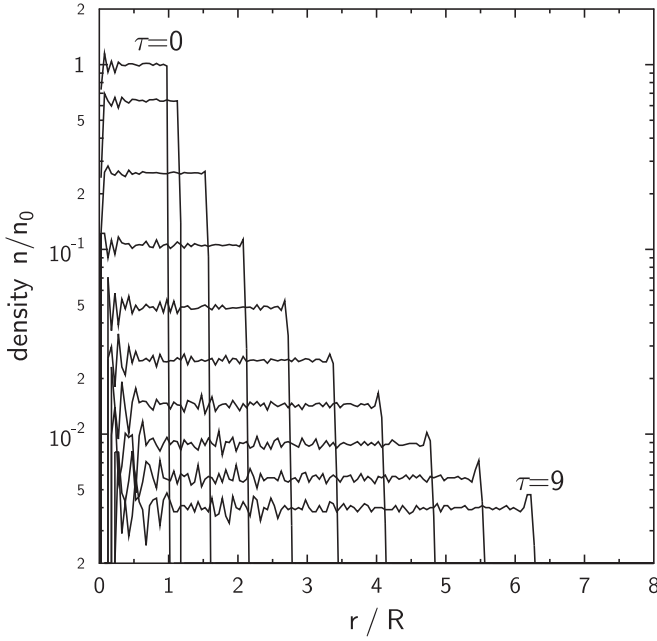


FIG. 4. Expansion of a Coulomb ball ($N = 2^{16}$, $\lambda \rightarrow \infty$). The density profile remains homogeneous during the expansion.

The transit time of a sound wave is given by $T_t = R/c_s$ with a sound speed $c_s = \omega_0 \lambda$. Then the normalized transit time becomes $\tau_t = \omega_0 T_t = R/\lambda$. A small-amplitude wave would reach the center of a homogeneous sphere at $\tau_t = 40.3$, which compares with $\tau \approx 30\text{--}35$ for the large-amplitude wave in the present example.

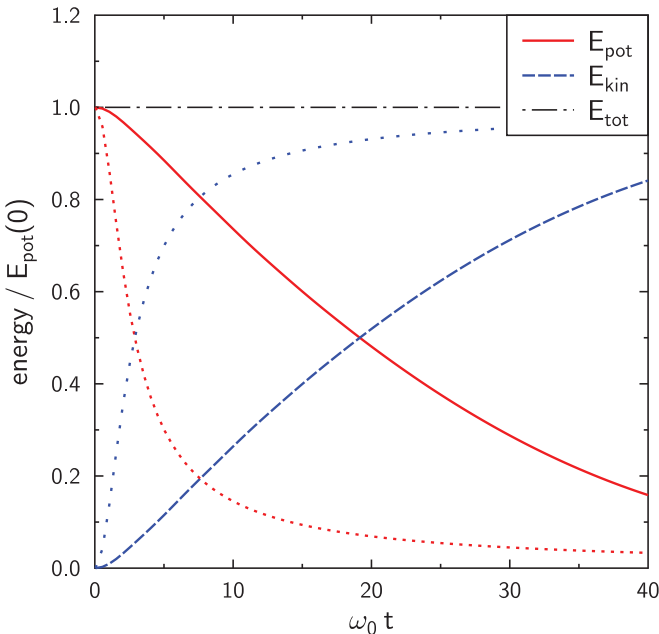


FIG. 5. (Color online) Evolution of the total potential energy (solid line) and kinetic energy (dashed line) in the Yukawa ball expansion ($N = 2^{16}$, $R/\lambda = 40.3$). The dotted curves represent the corresponding Coulomb ball expansion. All energies are normalized to the initial potential energy $E_{\text{pot}}(0)$.

B. Expansion of a Coulomb ball

For comparison, the same simulation program was used to explore the expansion of a Coulomb ball. Again we use $N = 2^{16}$ particles but the shielding factor is set to $\kappa = 0$, which gives the Coulomb limit. The result is shown in Fig. 4. The vertical axis is logarithmic to separate the density profiles more clearly.

It becomes immediately evident that the density profile of the Coulomb ball remains homogeneous during the expansion. For $\tau < 3$, the expansion is still governed by an increasing speed. For $\tau \geq 3$, the expansion speed has reached a nearly constant value and the density decays as $n(t) \propto t^{-3}$, accordingly.

C. Energy evolution

The evolution of the total potential and kinetic energy of the Yukawa ball with $N = 2^{16}$ particles are shown in Fig. 5. The energies are normalized by the initial potential energy $E_{\text{pot}}(0) = \sum_{i \neq j} q \Phi_Y(r_{ij})$ with the Yukawa potential from Eq. (6). The total energy at $\tau = 40$ is $E_{\text{tot}} = 0.9997 E_{\text{pot}}(0)$, which is a remarkably good value for the single-precision arithmetic in the fast N -body routine. The potential energy of the Yukawa ball has dropped to the $1/e$ value at $\tau_0 = 25.6$. For comparison, the Coulomb expansion is considerably faster with $\tau_0 = 4.1$.

D. Density profile evolution

The long-time evolution of the density profile of the Yukawa ball with $N = 2^{16}$ particles is shown in Fig. 6.

At $\tau = 10$ only the outer layers have separated from the bulk. The dotted box indicates the initial configuration, which has a 3% smaller density than the ideal normalized density $n/n_0 = 1$ with $n_0 = 3N/(4\pi R^3)$. This difference is caused by the arbitrariness in the definition of the proper “surface” of a discrete arrangement of particles. To minimize the initial correlation energy, we had chosen the procedure described at the end of Sec. IV with a radius of the confining cavity of $R + 0.5a_{\text{WS}}$.

At $\tau = 10$ only particles in the outer layer have gained energy from the repulsion by inner particles. This outer layer is subsequently blown off and moves at higher radial speed than particles that start from an inner layer, as can be seen in the energy distribution at $\tau = 30$.

At $\tau = 30$, the rarefactive wave has nearly reached the center of the sphere. At this time, the density profile has an approximately triangular shape and the Yukawa ball has reached a radius of ≈ 2.1 . At $\tau = 50$, the total potential energy of the Yukawa ball is only 10% of its initial value. Therefore, the further expansion of the low-density outer part of the expanding cloud is simply a ballistic radial motion. This becomes evident from the fact that the kinetic energy of the particles at the leading edge remains practically constant for $50 < \tau < 100$.

The triangular density profile at $\tau = 50$ gradually transforms into a plateau at $\tau = 100$. One could imagine that this transformation is a rarefactive wave that propagates outward after being reflected at the center.

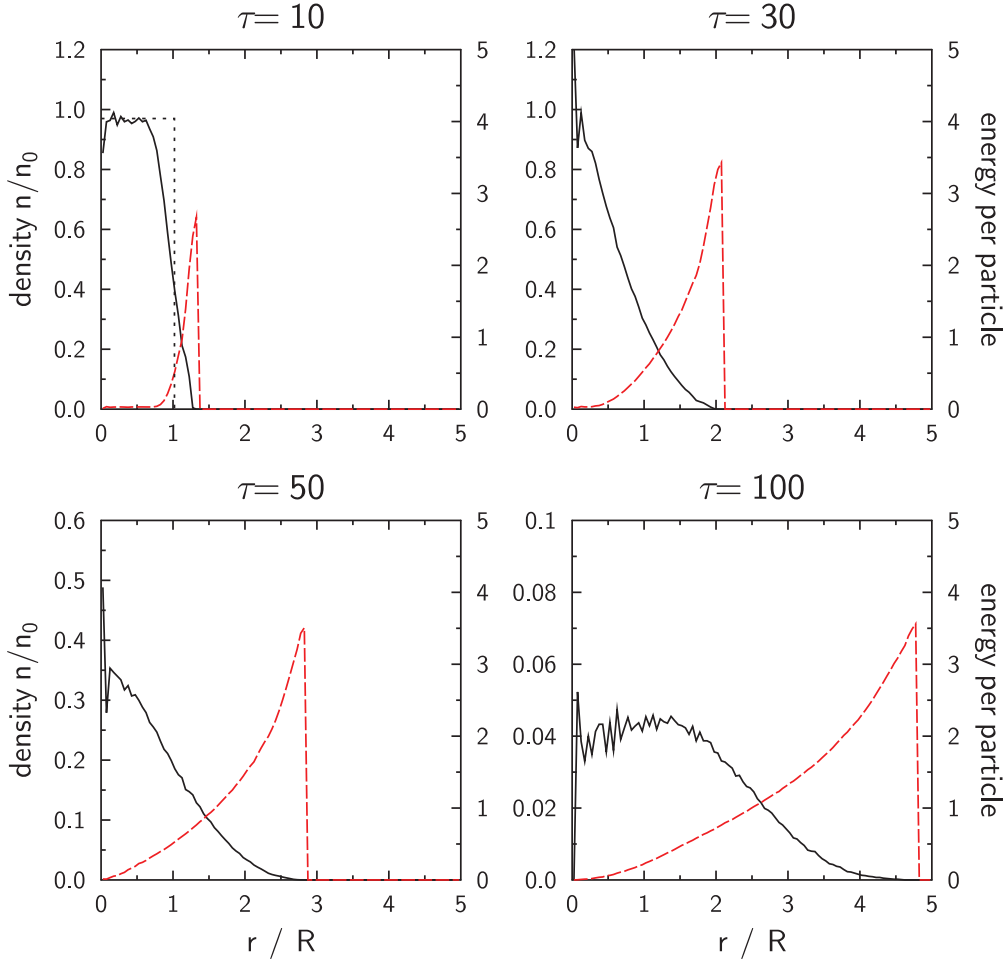


FIG. 6. (Color online) Long-time expansion of a Yukawa ball of initial radius R (dotted box) up to $\tau = 100$ ($N = 2^{16}$, $R/\lambda = 40.3$). Density profiles (solid lines) and kinetic energy per particle (red dashed lines).

Since the blow-off of the outer shell of a large Yukawa ball carries away a substantial fraction of the total kinetic energy it is tempting to compare the decay time τ_0 of a Yukawa ball with the dynamics of a test particle at the surface. The potential energy of a particle of charge q at the surface $r = R$ is obtained from Eq. (B8), which for $R/\lambda \gg 1$ approaches the limit $E_{\text{pot},1} = (1/2)m\omega_0^2\lambda^2$. When this potential energy is converted to kinetic energy of the test particle, its speed $v = \omega_0\lambda$ is just the sound speed.

Therefore, the characteristic time for the expansion process can be defined as the (absolute) transit time through the characteristic size R , $T_t = R/v$. The normalized transit time is then $\tau_t = R/\lambda$, i.e., the transit time of the rarefactive wave in Sec. VA. In Fig. 7 the decay times of Yukawa balls with fixed number $N = 2^{16}$ but varying R/λ are compared with this transit time. The Coulomb decay time from Fig. 5 is marked by the short dashed line. For $R/\lambda \geq 5$ the linear increase of the asymptotic behavior is well reproduced. A best fit gives $\tau_0 \approx 0.7\tau_t$.

Surprisingly, for $R/\lambda < 1$, the Coulomb limit is not monotonically approached. Rather, a minimum decay time of a Yukawa ball is found at $R/\lambda = 1$ with 68% of the Coulomb decay time.

VI. THE INFLUENCE OF COLLISIONS ON THE EXPANSION OF A YUKAWA BALL

We now investigate the effects of gas atom collisions on the microparticles during the expansion. Two effects are taken into account in our Langevin-MD simulation: the random forces due to the impingement of gas molecules and the friction as the solid particles move through the gas. We perform our simulations for varying values of the gas friction coefficient γ , which we express in the dimensionless form $\nu = \gamma/\omega_0$. A uniform Yukawa ball containing $N = 2^{16}$ particles is assumed again to be confined in an equilibrium by an external force, which is suddenly switched off at $\tau = 0$ to begin the expansion.

We first investigate the blow-off of the outermost layer. For this purpose, we choose a representative sample of 500 randomly selected particles from the outermost bin of the initial density histogram. The long-term evolution up to $\tau = 400$ of the mean radial position of this group is shown in Fig. 8 for the collisionless and two collisional cases.

In the collisionless case, the trajectory becomes a straight line for $\tau > 50$. This is the ballistic motion of this leading group discussed in the previous section. In the collisional cases, the particle speed diminishes. The trajectory, however, has not the limited range that is known for initially

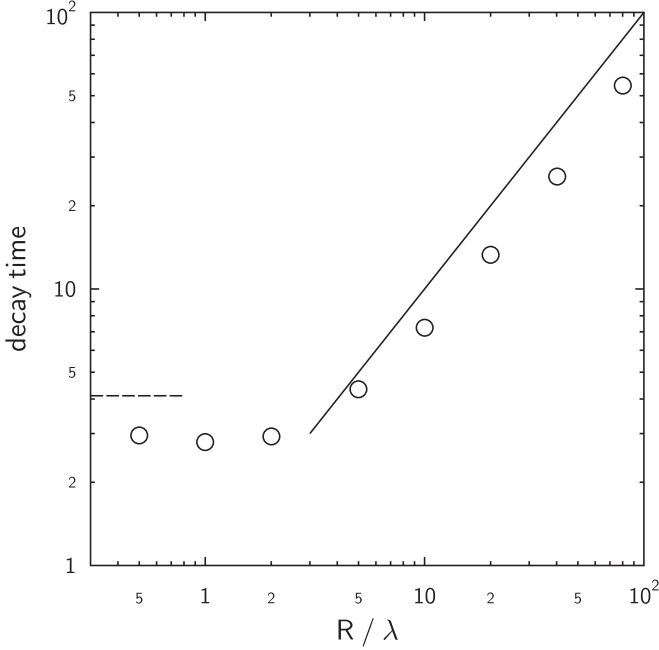


FIG. 7. Decay time (in normalized units $\tau = \omega_0 t$) of the Yukawa ball as a function of the shielding strength R/λ in comparison with the normalized transit time $\tau_t = R/\lambda$ (full line). The Coulomb decay time is given by the short dashed line.

monoenergetic particles in a medium with velocity-dependent friction, such as the famous α particles in air. Rather, the expansion of the outer layer seems to be governed by a continuously acting mechanism that is governed by a force equilibrium between frictional drag applied by the gas and a repulsive electric force from the inner particles.

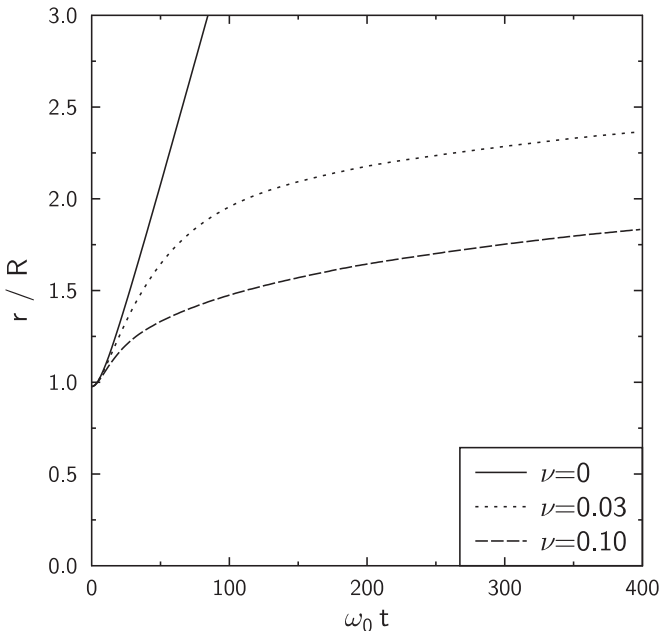


FIG. 8. Mean trajectory of 500 randomly selected particles in the outermost bin of the density histogram in collisionless and collisional expansions of a Yukawa ball ($N = 2^{16}$, $R/\lambda = 40.3$).

We first consider the case of weak friction, $\nu = 0.03$. As in the collisionless case, the expansion begins with a blow-off of the outer layer (Fig. 9, $\tau = 10$). The inward propagation of the rarefactive wave becomes evident at $\tau = 20$. The rarefactive wave reaches the center at $\tau \approx 30$ and a triangular profile similar to the collisionless case is found. Initially, the kinetic energy is concentrated in the outermost shell. Because the friction is velocity-dependent, the fastest particles experience the strongest deceleration, which can be seen in the height reduction of the initial sharp peak at the leading edge.

While, in the collisionless case, the speed of the outer layer increased until $\tau = 50$, in the present weakly damped situation the outer layer suffers a reduction of the peak energy by a factor of ≈ 5 . Moreover, the radial distribution of kinetic energy becomes a convex function, whereas it was concave in Fig. 6.

For larger friction, $\nu = 0.1$, the rarefactive wave is still seen, but after passing the triangular state at $\tau = 30$, the density profile rapidly evolves into a kind of inverted parabola at $\tau = 100$ (Fig. 10) and continuously expands while maintaining this shape. This observation can be confirmed by a simple model.

A large Yukawa ball consisting of a set of nested shells and being confined in a potential trap has a simple static construction principle [30]. Because we consider the limit $R/\lambda \gg 1$, each shell experiences a repulsive force from its immediate neighbors, which gives a net outward-directed force that is proportional to the density gradient. This net force is balanced by the restoring force from the trap. Therefore, a parabolic confinement leads to a density profile that consists of an inverted parabola plus an offset.

The same local approximation can be used to derive a simple analytic model for the expansion against friction. For this purpose, we assume that the instantaneous electric field from neighboring shells is proportional to the density gradient. In the collisional case the velocity \vec{v} of a microparticle is mobility-limited:

$$\vec{v} = -\mu \vec{E}(x) = -A \vec{\nabla} n(x). \quad (13)$$

This is not Fick's law for diffusion, which states that $n \vec{v} = -D \vec{\nabla} n$. Rather, combining Eq. (13) with the continuity equation $\partial n / \partial t + \vec{\nabla} \cdot (n \vec{v}) = 0$, we obtain a nonlinear differential equation for the density evolution

$$\frac{\partial n}{\partial t} = \frac{A}{2} \Delta(n^2), \quad (14)$$

with the Laplacian Δ . This is a special case of the ‘‘porous medium equation’’ (PME) $\partial n / \partial t = \Delta(n^m)$ [31], which allows arbitrary exponents $m > 1$ and describes nonlinear diffusion processes. The solutions $n(r, t)$ of this equation are known as ‘‘Barenblatt profiles’’ [32], which undergo a selfsimilar evolution with characteristic exponents. For $m = 2$ and a spherically symmetric expansion the solution has the form

$$n(x, t) = t^{-3/5} [C - kx^2 t^{-2/5}]_+. \quad (15)$$

The index ‘‘+’’ means that only positive values of the expression in brackets are valid. For any fixed time, the profile has the shape of an inverted parabola. This model makes three predictions, which we can test in the simulation results: (1) the profile is always an inverted parabola, (2) the maximum density decays $\propto t^{-3/5}$, and (3) the free boundary of the particle cloud expands as $t^{1/5}$.

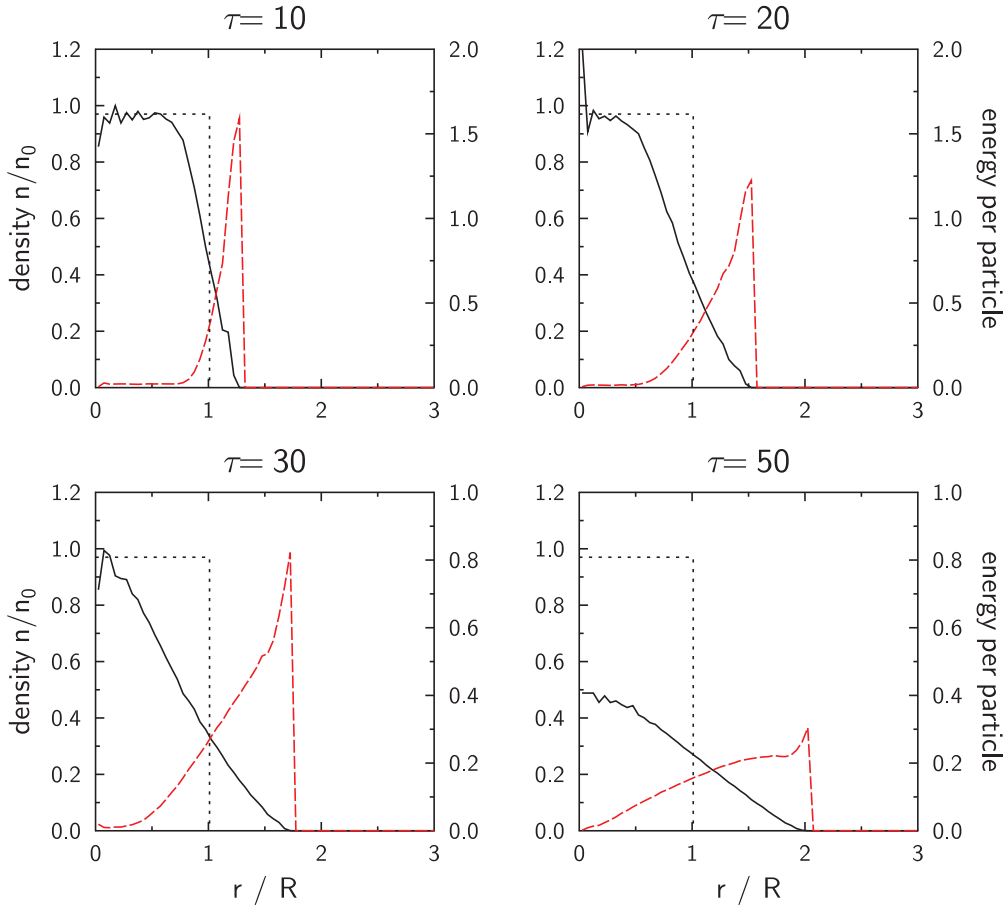


FIG. 9. (Color online) Early evolution of the density profile (solid line) and kinetic energy per particle (red dashed line) in the weakly collisional case ($\nu = 0.03$, $N = 2^{16}$, $R/\lambda = 40.3$). The dotted box indicates the initial density profile.

The first test is performed in Fig. 10, where the simulation results for the long-term evolution are compared with best

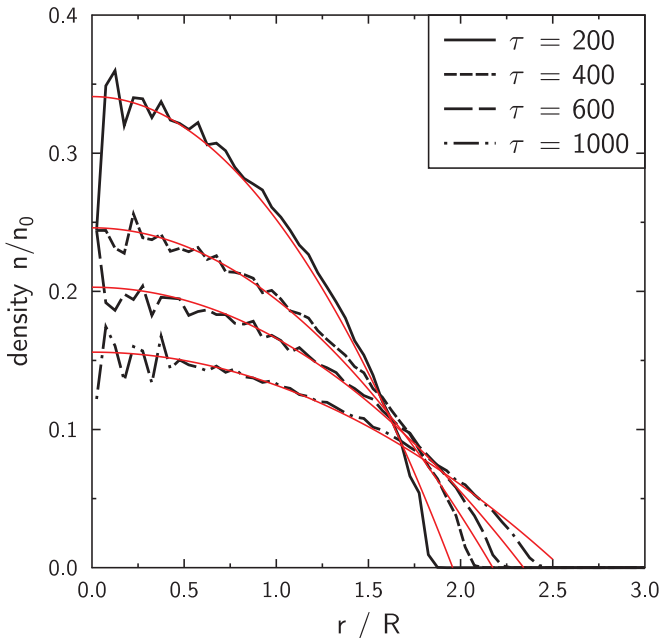


FIG. 10. (Color online) Fit of the density profiles for $\nu = 0.1$, $N = 2^{16}$, $R/\lambda = 40.3$ by Barenblatt profiles (fine red lines).

fits by inverted parabolas. The close agreement confirms the validity of the exponent $m = 2$ in the PME, which resulted from the assumption of a local mobility [Eq. (13)].

The other tests are made in Fig. 11, where the height and width of the best-fit parabolas are shown. The decay of the maximum density is close to the $t^{-3/5}$ law and the expansion is very slow and follows nearly the $t^{1/5}$ law. In conclusion, the collisional expansion of a Yukawa ball approaches the limit of nonlinear diffusion described by the PME for $m = 2$.

VII. SUMMARY AND CONCLUSIONS

The dynamics of Coulomb explosions was shortly summarized and the self-similarity of the expansion process became evident for the collisionless and the collisional case. In particular, an initially homogeneous density profile stays homogeneous for all times. For Yukawa balls we use the terminology “expansion” to distinguish the process from an explosive process that acts simultaneously in all parts of the system.

In a system of stratified layers of “Yukawa matter” the collisionless expansion is characterized by an ablation process, in which the outermost layer is blown off at a higher speed than subsequent layers. The ablation of subsequent layers is delayed by a time that is given by the propagation speed of a rarefactive wave, $v = \omega_0 \lambda$. For the points of weak displacement, a linear

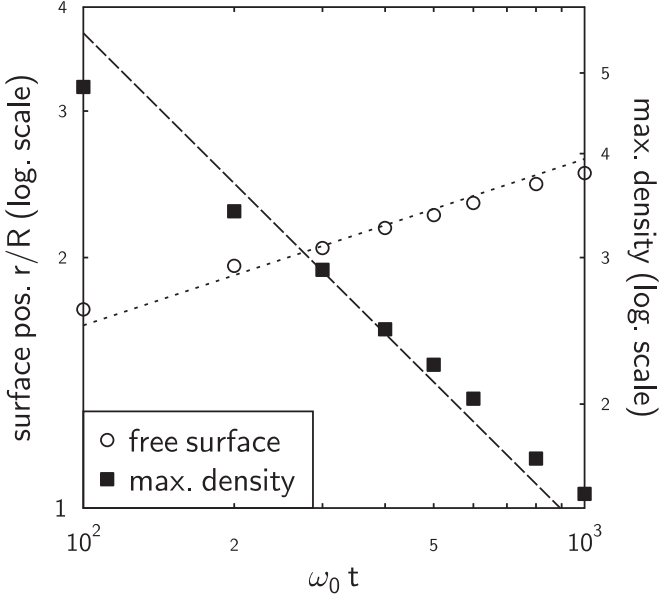


FIG. 11. Test of the Barenblatt model for nonlinear diffusion. Expansion of the free surface (circles) in comparison with power law $\propto (\omega_0 t)^{1/5}$ (dotted line). Decay of the central maximum (squares) in comparison with power law $\propto (\omega_0 t)^{-3/5}$ (dashed line).

rarefactive wave is found to propagate exactly at the sound velocity for a system of equidistant sheets interacting by Yukawa forces. This sound speed is not the dust acoustic wave speed, which describes weakly coupled systems, but the long-wavelength limit of compressional phonons [25].

The electric field and potential for “Yukawa bubbles,” solid Yukawa spheres, and spherical cavities in an extended (homogeneous) medium of Yukawa particles were derived. The potential of a Yukawa cavity can be used to confine a homogeneous system of Yukawa simulation particles and is part of an “annealing” routine that allows us to prescribe a proper coupling factor Γ for the start configuration. The methods for MD simulations in the collisionless and collisional case were described in detail.

The fundamental processes remain similar for spherical objects, as could be demonstrated by MD simulations of collisionless systems. The large amplitude rarefactive wave reaches the center of the sphere at $\tau \approx 30\text{--}35$, which is close to the predicted transit time of a linear wave, $\tau_t = R/\lambda = 40.3$, in a system of $N = 2^{16}$ particles.

The decay time of a Yukawa ball can be defined as the $1/e$ value in the decay of the total potential energy. After this time, the particles from the outer layer perform a ballistic expansion, which can be seen as the constant speed of the free boundary of the density profile and agrees with the constant kinetic energy of this group. The decay time of a large system is determined by the speed of the particles in the outermost layer, which is just the sound speed. Therefore, the decay time of the total potential energy in large Yukawa balls is of the order of the transit time of the rarefactive wave to reach the center.

In the collisional case, the early evolution of the Yukawa ball is still governed by the blow-off of the outer layer and the inward propagation of a rarefactive wave. For large R/λ and in the mobility-dominated regime, the motion of a dust

particle is determined by the local electric field. This leads to a nonlinear diffusion process that can be described by the PME and leads to self-similar Barenblatt profiles and power-law behavior. In this way, the collective expansion of a collisional Yukawa system ends up in a nonlinear diffusion process.

Again, the local-field approximation gives a simple explanation of the underlying physical process. It had been the key to understanding the density profile of a Yukawa ball confined in a potential trap [30]. Here, it governs the force balance between frictional drag and electric repulsion between the charged particles that drives the nonlinear diffusion process.

ACKNOWLEDGMENTS

A.P. gratefully acknowledges support by Deutsche Forschungsgemeinschaft within the Transregional Collaborative Research Centre TR24 “Fundamentals of Complex Plasmas” Project A2 and by DLR (Contract No. 50WM1139). J.G. was supported by NASA and the National Science Foundation.

APPENDIX A: THE SOUND SPEED IN A SET OF CHARGED PLANES

We consider a system of plane sheets of surface charge density σ at positions $z_j = j \Delta z + \zeta_j$, which interact by a shielded electric field $E(z_n) = (\sigma/2\epsilon_0) \sum_{j \neq n} \text{sgn}(z - z_j) \exp(-|z - z_j|/\lambda)$. Assuming a wavelike displacement $\zeta(z) = \zeta_0 \exp[-i(kz - \omega t)]$ and setting $\bar{\kappa} = \Delta z/\lambda$, the dispersion relation for longitudinal waves reads

$$\omega^2 = 2\omega_0^2 \bar{\kappa} \sum_{j=1}^{\infty} \exp(-j\bar{\kappa}) \sin^2 \left(j \frac{k\Delta z}{2} \right). \quad (\text{A1})$$

In the long wavelength limit ($k \rightarrow 0$), the dispersion is acoustic $\omega \propto k$ and the phase velocity equals the group velocity. The sound speed then becomes

$$c_s = \omega_0 \lambda \left(\frac{\bar{\kappa}^3}{2} \sum_{j=1}^{\infty} j^2 e^{-j\bar{\kappa}} \right)^{1/2}. \quad (\text{A2})$$

It turns out that for experimental situations, which typically have $\bar{\kappa} < 2$, the square-root factor is practically equal to 1 within 2% accuracy. Therefore, the group velocity is practically $v_g = \omega_0 \lambda$.

APPENDIX B: ELECTRIC FIELD AND POTENTIAL OF NESTED SPHERICAL SHELLS

We first consider thin spherical shells (“bubbles”) of radius R consisting of particles with Yukawa interaction and use a mean-field approach. The electric potential inside a single shell of radius R and surface charge density σ is given in spherical coordinates by

$$\Phi(r) = \frac{\sigma}{2\epsilon_0} \int_0^\pi \frac{R^2 \sin \theta}{s(r, \theta)} \exp \left(-\frac{s(r, \theta)}{\lambda} \right) d\theta, \quad (\text{B1})$$

with $s(r, \theta) = (R^2 + r^2 - 2Rr \cos \theta)^{1/2}$. The resulting potential and electric field are

$$\Phi_{\text{in}}(r) = \frac{\sigma}{\epsilon_0} R e^{-R/\lambda} \frac{\lambda}{r} \sinh\left(\frac{r}{\lambda}\right), \quad (\text{B2})$$

$$E_{\text{in}}(r) = \frac{\sigma}{\epsilon_0} e^{-R/\lambda} \frac{R}{r} \left[\frac{\lambda}{r} \sinh\left(\frac{r}{\lambda}\right) - \cosh\left(\frac{r}{\lambda}\right) \right]. \quad (\text{B3})$$

Outside of the spherical shell the electric potential and field are given by

$$\Phi_{\text{out}}(r) = \frac{\sigma}{\epsilon_0} R \sinh\left(\frac{R}{\lambda}\right) \frac{\lambda}{r} e^{-r/\lambda}, \quad (\text{B4})$$

$$E_{\text{out}}(r) = \frac{\sigma}{\epsilon_0} \sinh\left(\frac{R}{\lambda}\right) \frac{R}{r} \left(\frac{\lambda}{r} + 1 \right) e^{-r/\lambda}. \quad (\text{B5})$$

For large values of R/λ , the electric field near the spherical shell approaches the behavior of a plane shell, $E(r - R) \approx \text{sgn}(r - R)(\sigma/2\epsilon_0) \exp(-|r - R|/\lambda)$ [see Eq. (7)].

The electric potential outside of a solid sphere of Yukawa matter can then be obtained by integration over a set of nested shells and we obtain for $r \geq R$

$$\Phi_{\text{sph}}(r) = \frac{\rho_c \lambda^2}{\epsilon_0} \left[\frac{R}{\lambda} \cosh\left(\frac{R}{\lambda}\right) - \sinh\left(\frac{R}{\lambda}\right) \right] \frac{\lambda}{r} e^{-r/\lambda}, \quad (\text{B6})$$

$$E_{\text{sph}}(r) = \frac{\rho_c \lambda}{\epsilon_0} \left[\frac{R}{\lambda} \cosh\left(\frac{R}{\lambda}\right) - \sinh\left(\frac{R}{\lambda}\right) \right] \times \left(\frac{\lambda^2}{r^2} + \frac{\lambda}{r} \right) e^{-r/\lambda}, \quad (\text{B7})$$

with the initial mean charge density $\rho_c = 3Nq/(4\pi R^3)$. For large values of R/λ the potential attains the limiting case

$$\Phi_{\text{sph}}(r) \approx \frac{3}{2} \frac{\lambda^2}{R^2} \frac{Nq}{4\pi \epsilon_0 r} e^{(r-R)/\lambda}. \quad (\text{B8})$$

The surface potential of a Yukawa sphere is used in the discussion of the potential energy of a test particle in the surface layer in Sec. V.

With a similar integration over nested shells we obtain the potential inside a spherical cavity of radius R of an infinitely extended region of Yukawa matter, which for $r \leq R$ reads

$$\Phi_{\text{cav}}(r) = \frac{\rho_c \lambda^2}{\epsilon_0} \left(\frac{R}{\lambda} + 1 \right) e^{-R/\lambda} \frac{\lambda}{r} \sinh\left(\frac{r}{\lambda}\right), \quad (\text{B9})$$

$$E_{\text{cav}}(r) = \frac{\rho_c \lambda}{\epsilon_0} \left(\frac{R}{\lambda} + 1 \right) e^{-R/\lambda} \times \frac{\lambda}{r} \left[\sinh\left(\frac{r}{\lambda}\right) - \frac{\lambda}{r} \cosh\left(\frac{r}{\lambda}\right) \right]. \quad (\text{B10})$$

This cavity potential is a very useful result for the confinement of a homogeneous distribution of Yukawa particles with a minimum of correlation energy that can be used as the start situation for our MD simulation (Sec. IV).

-
- [1] O. Arp, D. Block, A. Piel, and A. Melzer, *Phys. Rev. Lett.* **93**, 165004 (2004).
- [2] O. Arp, D. Block, M. Klindworth, and A. Piel, *Phys. Plasmas* **12**, 122102 (2005).
- [3] M. Bonitz, D. Block, O. Arp, V. Golubnychiy, H. Baumgartner, P. Ludwig, A. Piel, and A. Filinov, *Phys. Rev. Lett.* **96**, 075001 (2006).
- [4] C. Henning, H. Baumgartner, A. Piel, P. Ludwig, V. Golubnychiy, M. Bonitz, and D. Block, *Phys. Rev. E* **74**, 056403 (2006).
- [5] D. Block, M. Kroll, O. Arp, A. Piel, S. Käding, A. Melzer, C. Henning, H. Baumgartner, P. Ludwig, and M. Bonitz, *Plasma Phys. Control. Fusion* **49**, B109 (2007).
- [6] D. Block, S. Käding, A. Melzer, A. Piel, H. Baumgartner, and M. Bonitz, *Phys. Plasmas* **15**, 040701 (2008).
- [7] A. Melzer, S. Käding, D. Block, and A. Piel, *J. Phys. Condens. Matter* **20**, 404204 (2008).
- [8] A. Melzer, B. Buttenschön, T. Miksch, M. Passvogel, D. Block, O. Arp, and A. Piel, *Plasma Phys. Control. Fusion* **52**, 124028 (2010).
- [9] H. Baumgartner, D. Block, and M. Bonitz, *Contrib. Plasma Phys.* **49**, 281 (2009).
- [10] A. Schella, T. Miksch, A. Melzer, J. Schablinski, D. Block, A. Piel, H. Thomsen, P. Ludwig, and M. Bonitz, *Phys. Rev. E* **84**, 056402 (2011).
- [11] A. Melzer, A. Schella, T. Miksch, J. Schablinski, D. Block, A. Piel, H. Thomsen, H. Ählert, and M. Bonitz, *Contrib. Plasma Phys.* **52**, 795 (2011).
- [12] A. Barkan and R. L. Merlino, *Phys. Plasmas* **2**, 3261 (1995).
- [13] A. Melzer and J. Goree, in *Low Temperature Plasmas: Fundamentals, Technologies and Techniques*, 2nd ed., edited by R. Hippler, H. Kersten, M. Schmidt, and K. Schoenbach (Wiley-VCH, Weinheim, 2008), Chap. 6.
- [14] V. Saxena, K. Avinash, and A. Sen, *Phys. Plasmas* **19**, 093706 (2012).
- [15] T. Antonova, C. R. Du, A. V. Ivlev, B. M. Annaratone, L. J. Hou, R. Kompaneets, H. M. Thomas, and G. E. Morfill, *Phys. Plasmas* **19**, 093709 (2012).
- [16] A. V. Ivlev, *Phys. Rev. E* **87**, 025102 (2013).
- [17] R. Wester, F. Albrecht, M. Grieser, L. Knoll, D. Schwalm, A. Wolf, A. Baer, J. Levin, Z. Vager, and D. Zajfman, *Nucl. Instrum. Methods A* **413**, 379 (1998).
- [18] T. Ditmire, T. Donnelly, R. W. Falcone, and M. D. Perry, *Phys. Rev. Lett.* **75**, 3122 (1995).
- [19] E. L. Clark, K. Krushelnick, M. Zepf, F. N. Beg, M. Tatarakis, A. Machacek, M. I. K. Santala, I. Watts, P. A. Norreys, and A. E. Dangor, *Phys. Rev. Lett.* **85**, 1654 (2000).
- [20] K. Nishihara, H. Amitani, M. Murakami, S. V. Bulanov, and T. Z. Esirkepov, *Nucl. Instrum. Methods A* **464**, 98 (2001).
- [21] S. Sakabe, S. Shimizu, M. Hashida, S. Sato, T. Tsuyukushi, K. Nishihara, S. Okihara, T. Kagawa, Y. Izawa, K. Imasaki, and T. Iida, *Phys. Rev. A* **69**, 023203 (2004).
- [22] M. Grech, R. Nuter, A. Mikaberidze, P. Di Cintio, L. Gremillet, E. Lefebvre, U. Saalman, J. M. Rost, and S. Skupin, *Phys. Rev. E* **84**, 056404 (2011).

- [23] I. Last, I. Schenk, and J. Jortner, *J. Chem. Phys.* **107**, 6685 (1997).
- [24] V. Y. Bychenkov and V. F. Kovalev, *Plasma Phys. Rep.* **31**, 178 (2005).
- [25] G. Kalman, M. Rosenberg, and H. E. DeWitt, *Phys. Rev. Lett.* **84**, 6030 (2000).
- [26] L. Nyland, M. Harris, and J. Prins, in *GPU Gems 3*, edited by H. Nguyen (Addison-Wesley, Boston, 2007), Chap. 31.
- [27] A. T. Brünger, C. Brooks, and M. Karplus, *Chem. Phys. Lett.* **105**, 495 (1984).
- [28] C. E. Simien, Y. C. Chen, P. Gupta, S. Laha, Y. N. Martinez, P. G. Mickelson, S. B. Nagel, and T. C. Killian, *Phys. Rev. Lett.* **92**, 143001 (2004).
- [29] A. Denning, S. D. Bergeson, and F. Robicheaux, *Phys. Rev. A* **80**, 033415 (2009).
- [30] A. Piel, O. Arp, D. Block, I. Pilch, T. Trottenberg, S. Käding, A. Melzer, H. Baumgartner, C. Henning, and M. Bonitz, *Plasma Phys. Control. Fusion* **50**, 124003 (2008).
- [31] J. L. Vazquez, *The Porous Medium Equation* (Oxford University Press, Oxford, 2007).
- [32] G. I. Barenblatt, *Prikl. Mat. Mekh.* **16**, 67 (1952).